Mean, variability and trend of Southern Ocean wind stress: Role of wind fluctuations

Xia Lin[1,2], Xiaoming Zhai[2], Zhaomin Wang[3] and David R. Munday[4]

[1]Polar Climate System and Global Change Laboratory, Nanjing University of Information Science and Technology, Nanjing, China

[2]Centre for Ocean and Atmospheric Sciences, School of Environmental Sciences, University of East Anglia, Norwich, United Kingdom

[3]College of Oceanography, Hohai University, Nanjing, China

[4]British Antarctic Survey, Cambridge, United Kingdom

Correspondence to: Xiaoming Zhai (Xiaoming.Zhai@uea.ac.uk) and Zhaomin Wang (Zhaomin.Wang@hhu.edu.cn).

Abstract

The Southern Ocean (SO) surface westerly wind stress plays a fundamental role in driving the Antarctic Circumpolar Current and the global meridional overturning circulation. Here we investigate the contributions of atmospheric wind fluctuations to the mean, variability and trend of SO wind stress over the last four decades using NCEP and ERA-Interim reanalysis products. Including wind variability at synoptic frequencies (2-8 days) and higher in the stress calculation is found to increase the strength of the mean SO wind stress by almost 40% in both reanalysis products. The Southern Annular Mode index is found to be a good indicator for the strength of the mean wind and mean wind stress, but not as good an indicator for wind fluctuations, at least for the chosen study period. Large discrepancies between reanalysis products emerge regarding the contributions of wind fluctuations to the strengthening trend of SO wind stress. Between one-third and half of the stress trend in NCEP can be explained by the increase in the intensity of wind fluctuations, while the stress trend in ERA-Interim is due entirely to the increasing strength of the mean westerly wind. This trend discrepancy may have important climatic implications since the sensitivity of SO circulation to wind stress changes depends strongly on how these stress changes are brought about. Given the important role of wind fluctuations in shaping the SO wind stress, studies of the SO response to wind stress changes need to account for changes of wind fluctuations in the past and future.

1. Introduction

The Southern Hemisphere (SH) surface westerly wind stress is a major forcing for driving the Antarctic Circumpolar Current (ACC) and upwelling of deep waters in the Southern Ocean (SO). The SH westerly wind stress has strengthened significantly over the last few decades and is projected to continue to do so in the future, which may have important implications for the global climate system via modulating the rate at which the SO uptakes heat and carbon (e.g. Thompson and Solomon 2002; Le Quéré et al. 2008; Marshall and Speer 2012; Wang et al. 2015; Wang et al. 2017). The strength of the SO wind stress is found to be closely related to the phase of the Southern Annual Mode (SAM), the dominant mode of atmospheric variability in the SH, with wind stress being stronger (and also poleward-shifted) during the positive phase of the SAM (e.g. Marshall 2003; Swart and Fyfe 2012). However, the SAM index is often defined based on the monthly-, seasonal- or annual-mean zonal sea level pressure difference between 40^{o}S and 65^{o}S (Gong and Wang 1999), and as such is a measure of the monthly-, seasonal-, or annual-mean strength of the westerly winds, rather than westerly wind stress. This could be problematic, since it is well known that the surface wind stress depends nonlinearly on surface wind velocity (e.g. Large et al. 1994; Zhai et al. 2012).

Due to the aforementioned nonlinear dependence of wind stress on surface wind, high-frequency wind fluctuations contribute to wind stress variability at both high and low frequencies (Zhai et al. 2012; Zhai 2013). For example, including wind fluctuations with time scales less than one month in the wind stress calculation significantly enhances the strength of the time-mean and seasonal-mean wind stress, particularly at mid and high latitudes. In turn this increases wind power input to the ocean general circulation by over 70% (Zhai et al. 2012; Wu et al. 2016). Therefore, studies on the changes of SO wind stress and their impact on the ocean need to take into account changes of not only the low-frequency (e.g. interannual) variability of the westerly jet but also wind fluctuations at much shorter time scales (e.g. days).

The strong positive trend of SO wind stress seen in observations, as well as atmospheric reanalysis products, has spurred a great deal of interest in how the SO responds to changes of surface wind stress forcing (e.g. Hallberg and Gnanadesikan 2001, 2006; Meredith and Hogg 2006; Böning et al. 2008; Farneti et al. 2010; Dufour et al. 2012; Munday et al. 2013; Bishop et al. 2016). This includes a number of steady-state sensitivity modeling studies where the mean SO wind stress is strengthened and/or shifted (e.g. Downes et al. 2011; Zhai and Munday 2014; Spence et al. 2014; Munday and Zhai 2015; Bishop et al. 2016; Hogg et al. 2017) as well as some observational and modelling studies of the transient response of the ACC and SO eddy field to changes of the SAM (e.g. Meredith and Hogg 2006; Screen et al. 2009; O'Kane et al. 2013; Langlais et al. 2015). Two dynamical phenomena: eddy saturation (Straub 1993) and eddy compensation (Viebahn and Eden 2010), which refer to the loss and reduced sensitivity of ACC transport and SO meridional overturning circulation to wind stress changes respectively, emerge from model studies with resolved or permitted, rather than parameterized, mesoscale ocean eddies[1]. Model investigations into the eddy saturation and eddy compensation phenomena typically involve directly varying the magnitude of the mean wind stress in the SO. The underlying assumption of this approach is that the stress varies due to changes of the mean wind[2]. In reality, however, some of the observed and predicted wind stress changes may be brought about by changes in the variability of the atmospheric wind, owing to the nonlinear nature of the stress law (Zhai 2013).

[1] Non-eddy-resolving ocean models with a variable eddy parameterization coefficient are found to be capable of achieving partial eddy compensation (e.g. Farneti et al. 2010; Gent 2016).

[2] If the increase in the magnitude of the mean wind stress is a result of increased wind variability, there should be a concurrent increase in wind stress variability, but this is absent in sensitivity model experiments where the strength of the mean stress is directly varied (e.g. doubled). High-frequency wind stress fluctuations are known to be important in setting the surface mixed layer depth (e.g. Sui et al. 2003; Kamenkovich 2005; Zhou et al. 2018).

An exception to this common practice of directly varying the mean wind stress is a recent study by Munday and Zhai (2017), who investigated the impact of wind fluctuations on the sensitivity of SO stratification and circulation to wind stress changes. In their study, changes of the mean wind stress felt by the ocean were made through alteration of the wind variability, as opposed to the mean wind. Stronger wind variability is found to enhance near-surface energy dissipation and increase near-surface viscous and diffusive mixing (see also Jouanno et al. 2016; Sinha and Abernathey 2016). The increased vertical mixing deepens the surface mixed layer and results in a much greater sensitivity (more than doubled) of the SO meridional overturning circulation to the increased wind stress, when compared to equivalent experiments forced by changing the mean wind. This result has important implications for understanding the SO response to past and future wind stress changes, should changes in wind stress be brought about not only by changes of the mean wind but also by changes of wind variability. However, to our knowledge, there have been few studies (Zhai et al. 2012; Zhai 2013; Franzke et al. 2015) so far assessing the role of wind fluctuations in determining the mean, variability and trend of the observed wind stress in the SO. A number of studies exist on the changes of the SH storm track and cyclone activities (Simmonds and Keay 2000; Yin 2005; Grieger et al. 2014; Wang et al. 2016; Chang 2017). However, the link between changes in these synoptic atmospheric systems to changes in SO wind stress has not yet been made.

In this study, we use reanalysis data products to investigate the contributions of wind fluctuations on different time scales (6 hours to 2days, 2 to 8 days and 8 days to 1 year) to the mean, variability and trend of SO wind stress for the first time. The paper is organized as follows. We begin in section 2 by describing the reanalysis products and analysis methods used in this study. In Section 3, we first examine the effect of wind fluctuations on the time-mean and seasonal-mean wind stresses in the SO, and this is followed by an investigation of the contribution of wind fluctuations to wind stress differences between positive and negative

SAM years as well as their contribution to the observed strengthening trend of SO wind stress. Finally, section 4 provides a summary and some concluding remarks.

2. Data and Methods

2.1 Reanalysis data

Six-hourly 10-m wind fields from two widely-used atmospheric reanalysis products are analyzed in this study: NCEP-NCAR Reanalysis (NCEP R1; Kalnay et al. 1996) from the National Centers for Environmental Prediction and the ERA-interim Reanalysis (ERA-Interim; Dee et al. 2011) from the European Centre for Medium-Range Weather Forecasts. The NCEP R1 and ERA-Interim 10-m winds are provided on T62 (~210 km) and T255 (~80 km) grids respectively. Prior to 1979, the strength of the SH westerly jet in NCEP reanalysis product shows large spurious trends when compared to that derived from station data, owing to the gradual reduction of errors in the NCEP-simulated sea level pressure field at high southern latitudes (Hines et al. 2000; Marshall 2003). The situation is much improved with the introduction of the Television Infrared Observation Satellite (TIROS) Operational Vertical Sounder data into the reanalysis assimilation scheme after 1979. Because of this, we choose the analysis period in this study to be from January 1979 to December 2016. Previous studies find that although ERA-Interim is somewhat better in representing the characteristics of extratropical cyclones than NCEP R1 due to its higher spatial resolution (e.g. Jung et al. 2006; Tilinina et al. 2013), both reanalysis products tend to underestimate the dynamical intensity (e.g. maximum wind speed) of mesoscale atmospheric features such as mesocyclones and polar lows (Zappa et al. 2014; Verezemskaya et al. 2017). Figure 1 shows the comparison between the reanalysis winds and observed winds at four automatic weather stations from the SCAR READER project (Turner et al. 2004). The two reanalysis products reproduce reasonably well the salient features of wind variability at the four locations, but they both underestimate the amplitude of wind variability, most notably at high frequencies (e.g. 6 hours to 2 days).

Therefore, results from our study should be considered as a lower bound of the contribution of wind fluctuations to the SO wind stress, particularly at high frequencies.

The NCEP-DOE Reanalysis product (NCEP R2; Kanamitsu et al. 2002), an improved version of NCEP R1[3], and the Japanese 55-year Reanalysis product (JRA-55; Kobayashi et al., 2015) provided on the T319 (~63 km) grid, are also analyzed in this study. Since the results from NCEP R2 and JRA-55 are very similar to those from NCEP R1 and ERA-Interim except for the trend, we only include results from NCEP R2 and JRA-55 when comparing trends of SO wind stress among different reanalysis products.

2.2 SAM index

Here we use the station-based SAM index data from Marshall (2003; updated online). The SAM index is defined, following Gong and Wang (1999), as

$$\mathrm{SAM} = \mathrm{P}^*_{40°\mathrm{S}} - \mathrm{P}^*_{65°\mathrm{S}},$$

where $\mathrm{P}^*_{40°\mathrm{S}}$ and $\mathrm{P}^*_{65°\mathrm{S}}$ are the normalized monthly zonal-mean sea level pressure at 40°S and 65°S, respectively, obtained by averaging records from six stations at roughly 65°S and six stations at roughly 40°S. Readers are referred to Marshall (2003) for the locations of these stations as well as the criteria for choosing them. Note that the SAM index derived from NCEP and ERA-Interim reanalysis products are found to be in very good agreement with that derived from station data after 1979 (Thompson and Solomon 2002; Marshall 2003).

2.3 Wind stress

The zonal surface wind stress is calculated based on the bulk formula (Large et al. 1994),

$$\tau_x = \rho_a c_d |U_{10}| u_{10},$$

where τ_x is the surface zonal wind stress, u_{10} is the six-hourly 10-m zonal wind velocity and $|U_{10}|$ is the six-hourly 10-m wind speed from reanalysis data, $\rho_a = 1.223\ \mathrm{kg/m^3}$ is air density

[3] The improvements include an updated model with better physical parameterizations and fixing known data assimilation errors in NCEP R1.

at the sea surface, and c_d is the drag coefficient with $10^3 c_d = \frac{2.7}{|U_{10}|} + 0.142 + 0.0764|U_{10}|$. Here we do not explicitly investigate the role of the variable drag coefficient, although its effect is included in the wind stress calculations. Ocean surface velocity is not considered here in the stress calculation since its effect on the magnitude of SO wind stress is very small (a few percentage at most; see Wu et al. 2017). The zonal wind stress calculated from the bulk formula is slightly weaker than that provided in the reanalysis products owing to additional adjustments applied in the reanalysis models (Wesley Ebisuzali, NOAA, personal communication).

In order to quantify the effect of wind fluctuations on different time scales on the SO wind stress, we apply 2-day running mean, 8-day running mean and annual mean averaging to the original 6-hourly reanalysis wind field to filter out wind fluctuations that last less than 2 days, less than 8 days and less than one year, respectively. Threshold time scales of 2 days and 8 days are chosen here because atmospheric variability (e.g. wind and air temperature) on time scales of 2 to 8 days is generally thought to be associated with synoptic weather systems and baroclinic storm activities (e.g. Trenberth 1991; Inatsu and Hoskins 2004; Yin 2005). Figure 2 shows the magnitude of peak zonal-mean zonal wind stress in the SO as a function of the running mean time scale. The magnitude of peak zonal-mean zonal wind stresses in both NCEP R1 and ERA-Interim decreases rapidly with increasing running mean time scale up to synoptic time scales (~8 days) and then decreases much more gently afterwards. For example, increasing the running mean time scale to 10 days or 15 days leads to only 3% or 8% decrease in the calculated wind stresses, compared to those calculated from the 8-day running mean winds. Wind fluctuations on time scales of 2 to 8 days are calculated by taking the difference between the 2-day running mean and 8-day running mean wind fields. The 2-8 day filtered winds are then obtained by removing wind fluctuations on 2 to 8 days from the original 6-hourly wind field (Table 1). We recalculate the zonal wind stresses using these filtered winds (τ_{2d}, τ_{8d}, τ_{2-8d} and τ_{yr} from 2-day mean, 8-day mean, 2-8 day filtered and annual-mean winds respectively) and compare them with the zonal wind stress (τ_{6hr}) calculated from the 6-hourly reanalysis winds. For example, since wind fluctuations on 6 hours to 2 days are excluded in the calculation of τ_{2d}, the difference between τ_{6hr} and τ_{2d} can then be used to quantify the effect of including wind fluctuations on 6 hours to 2 days on the mean stress and its variability.

In addition to surface wind stress calculations, we also quantify kinetic energy of the wind field to help interpret some of the results shown in Section 3. Mean kinetic energy (MKE_{yr}) in each year is calculated from the annual-mean wind field, and eddy kinetic energy is calculated from wind fluctuations on time scales of 6 hours to 2 days (EKE_{2d}), 2 to 8 days (EKE_{2-8d}), 6 hours to 8 days (EKE_{8d}), and 6 hours to 1 year (EKE_{yr}), respectively (see Table 1 for the formulas). For example, EKE_{2d} is calculated using the difference between the 6-hourly and 2-day running mean wind fields. As such, EKE_{2d} represents kinetic energy associated with wind fluctuations on time scales of 6 hours to 2 days alone, and does not include the nonlinear cross term between fluctuations on 6 hours to 2 days and those on 2 days to 1 year.

3. Results

3.1 Mean

We first assess the effect of including wind fluctuations on different time scales on the mean wind stress in the SO. Figure 3 shows the 1979-2016 time-mean zonal wind stress calculated from the NCEP R1 (Figs. 3a to 3f) and ERA-Interim (Figs. 3g to 3l) reanalysis winds. Wind fluctuations are found to strengthen the mean wind stress almost everywhere in both reanalysis products, with the difference between multi-year mean τ_{6hr} and τ_{yr} often greater than τ_{yr} itself (Figs. 3a-c and 3g-i). This indicates that the annual mean wind alone can only explain ~1/2 of the annual mean wind stress. The significant contribution of wind fluctuations to the mean SO wind stress is a result of the large wind variability in this storm track region (Zhai 2013). Furthermore, the effect of including fluctuations on 6 hours to 8 days (Figs. 3a vs 3e and 3g vs 3k) is much larger than that of including fluctuations on 8 days to 1 year (Figs. 3e vs 3b and

3k vs 3h). Therefore, wind fluctuations on 6 hours to 8 days make a disproportionately large contribution to the mean stress. Quantitatively, including wind fluctuations in the stress calculation is found to increase the magnitude of peak zonal-mean wind stresses in NCEP R1 by about 109% (red vs yellow lines in Fig. 4a) and that in ERA-Interim by about 116% (Fig. 4c), with over 70% of both increases being contributed by wind fluctuations on 6 hours to 8 days (red vs purple lines in Figs. 4a and 4c). Including fluctuations on 6 hours to 2 days and those on 2 to 8 days appears to have a similar effect on the mean stress (overlapping green and cyan lines in Figs. 4a and 4c), with both acting to strengthen the peak mean wind stress by roughly 20%.

To understand the effect of including wind fluctuations on different time scales on the mean wind stress, it is instructive to examine the magnitude and spatial structure of the MKE and EKE. Figure 5 shows the time-mean zonal wind velocity, MKE and EKE calculated from wind fluctuations on different time scales from NCEP R1 (Figs. 5a-f) and ERA-Interim (Figs. 5g-l). The spatial patterns of the mean winds (Figs. 5a and 5g) are very similar to those of the mean wind stresses (Figs. 3a and 3g), with large values located in the South Indian Ocean sector. This similarity is also found in the zonal mean patterns of the mean wind and mean stress (solid red and dashed blue lines in Figs. 4a and 4c), with the peak values of both quantities found at 52 to 53^{o}S. Another striking feature in Figure 5 is the much broader and more uniform meridional (and zonal) distribution of the EKE, comparing to the MKE (Figs. 5b-c and 5h-i). The zonal-mean EKE increases gradually southward in the latitude band of 40^{o} to 60^{o}S and experiences somewhat sharper drops only north of ~40^{o}S and south of ~60^{o}S (Figs. 4b and 4d). This more or less uniform distribution of the EKE explains why the mean wind and mean stress peak at the same latitude: the strengthening of the mean stress owing to wind variability is largest where the mean wind is strongest.

EKE calculated from wind fluctuations on time scales of 6 hours to 2 days, 2 to 8 days, and 6 hours to 8 days is found to account for about 32%, 28%, and 71%, respectively, of the total EKE for both NCEP R1 (Fig. 4b) and ERA-Interim (Fig. 4d). These EKE percentages are broadly comparable to the percentage increases of the mean stress after including wind fluctuations on different time scales, demonstrating that the effect of wind variability on the strength of the mean stress via the nonlinear stress law depends on the magnitude of the wind variability. Stronger wind variability in ERA-Interim also contributes to the larger mean stress in ERA-Interim than NCEP R1 (red lines in Figs. 4a and 4c), although the mean winds in the two reanalysis products are comparable in strength (dashed blue).

For both reanalysis products, the zonal mean wind peaks in austral spring and autumn (dashed green and blues lines in Figs. 6a and c), while it shifts equatorward in austral summer (dashed red) and becomes weaker but broader in austral winter (dashed black). Interestingly, the zonal mean wind stress in austral winter (solid black) is greater than that in austral summer (solid red), even in the latitude band of 44^{o}S-56^{o}S where the mean wind is noticeably weaker in austral winter than in austral summer (dashed black vs dashed red). This paradox is explained by the pronounced seasonal cycle of the EKE in the SO (Figs. 6b and d), characterized by EKE being the largest in austral winter (dashed black) and smallest in austral summer (dashed red). Stronger wind variability in austral winter increases the magnitude of the mean stress much more significantly than that in austral summer, resulting in the larger mean stress seen in austral winter. It is worth pointing out that EKE is greater than MKE in the SO in all four seasons for both reanalysis products (Figs. 6b and d).

3.2 Variability

In this section, we investigate the role of wind fluctuations in determining wind stress differences between positive and negative SAM years. Here a year with SAM > 0.5 is defined as a positive SAM year and a year with SAM < -0.5 a negative SAM year (Fig. 7).

Figure 8 shows the mean stress, MKE_{yr} and EKE_{yr} in positive and negative SAM years calculated from NCEP R1 (Figs. 8a-h) and ERA-Interim reanalysis winds (Figs. 8i-p). Consistent with previous studies, both the mean wind and mean stress in positive SAM years (Figs. 8a and i) are found to be considerably stronger and also shifted poleward by a few degrees (Figs. 9a-b and d-e), with respect to those in negative SAM years (Figs. 8e and m). In contrast, the mean EKE_{yr} shows no statistically significant differences between positive and negative SAM years in both reanalysis products (Figs. 8d, h, i, p and 9c, f). One noticeable difference between NCEP R1 and ERA-Interim is the much larger spread of EKE_{yr} in NCEP R1 (Figs. 9c and f), indicating a stronger inter-annual variability of EKE_{yr} in the SO in this reanalysis product. There is a hint of a poleward shift of EKE_{yr} in positive SAM years in ERA-Interim (Fig. 9f). These results show that the SAM index is a good indicator of the strength of the mean wind and mean stress, but not as good an indicator for the strength of wind fluctuations, at least for our analysis period of 1979-2016.

To further assess the role of wind fluctuations in determining the wind stress differences seen between positive and negative SAM years, we recalculate the mean stress using a combination of the mean wind averaged over all the positive SAM years and wind fluctuations from each negative SAM year (Figs. 8b and j) and also using a combination of the mean wind averaged over all the negative SAM years and wind fluctuations from each positive SAM year (Figs. 8f and n). Remarkably, there is virtually no difference between the mean stress in positive SAM years and the mean stress calculated using a combination of the mean wind from positive SAM years and wind fluctuations from negative SAM years (Figs. 8a vs 8b and Figs. 8i vs 8j). The same is true for the mean stress in negative SAM years and the mean stress calculated using a combination of the mean wind from negative SAM years and wind fluctuations from positive SAM years (Figs. 8e-f and m-n). This result suggests that as far as the nonlinear stress law is concerned, it is the magnitude of wind fluctuations that matters for determining the magnitude of the mean stress, not whether wind fluctuations and the mean wind are dynamically linked. The result also shows that differences in the mean wind are the key cause for the differences in the mean stress found between positive and negative SAM years, although the presence of wind fluctuations significantly amplifies these mean stress differences; in the absence of wind fluctuations, the mean stress difference between positive and negative SAM years is much smaller (not shown). The situation in the SO appears to be in contrast to that at mid-latitude North Atlantic, where stronger westerly wind stress during years of positive North Atlantic Oscillation is found to be mostly a result of enhanced synoptic wind variability, rather than a stronger background mean wind (Zhai and Wunsch 2013).

3.3 Trend

We now assess the contribution of wind fluctuations to the strengthening trend of SO wind stress over the last four decades. Results from NCEP R2 and JRA-55 are also included here since they are significantly different from NCEP R1 and ERA-Interim.

The trends of the strength of SO wind stress during 1979-2016 are 0.00038 N m^{-2} yr^{-1} in NCEP R1 (Fig. 10a), 0.00067 N m^{-2} yr^{-1} in NCEP R2 (Fig. 10b) and 0.00023 N m^{-2} yr^{-1} in ERA-Interim (Fig. 10c), all significant at <1% level by T test, while no significant trend (<5%) is detected in JRA-55. This is consistent with the results in Thomas et al. (2015) who also found the largest trend of SO wind stress in NCEP R2 but no significant trend in JRA-55 for the period of 1980-2004. In order to separate out contributions from the mean wind and wind fluctuations to the wind stress trends found in the reanalysis products, we randomly reshuffle the annual-mean wind and wind fluctuations in each year over the whole 38-year period. First, the annual-mean wind fields are randomly reshuffled for 38 times. Each time a new time series of wind stress is calculated using a combination of the reshuffled annual-mean wind and unshuffled wind fluctuations. We then average the 38 time series of wind stress and find the trend of the averaged stress (black lines in Fig. 10). This new trend obtained by randomizing the annual-mean winds excludes the effect of changes of the annual-mean wind and thus enables us to see how the increased intensity of wind fluctuations with time contributes to the strengthening trend of the wind stress. Similarly, we randomly reshuffle wind fluctuations of each year 38 times, calculate 38 time series of wind stress using a combination of the reshuffled wind fluctuations and unshuffled annual-mean winds, and find the trend of the time series of the averaged stress (blue lines in Fig. 10). The new trend obtained by randomizing wind fluctuations excludes the effect of changing intensity of wind fluctuations, enabling us to see how the strengthening of the annual-mean wind contributes to the strengthening trend of the wind stress.

After randomizing the annual-mean winds over the last four decades, the trends of the strength of SO wind stress are 0.00014 N m^{-2} yr^{-1} for NCEP R1, 0.00034 N m^{-2} yr^{-1} for NCEP R2, and 0.00003 N m^{-2} yr^{-1} for ERA-Interim (black lines in Fig. 10), respectively. Importantly, the trends for both NCEP reanalysis products are significant at <5% level, whereas the trend for ERA-Interim is not statistically significant. Therefore, changes of wind fluctuations explain about one-third and half of the strengthening trend of Sothern Ocean wind stress in NCEP R1 and NCEP R2 respectively, but make no significant contribution in ERA-Interim. The positive wind stress trend in ERA-Interim is due entirely to the increase in the strength of the annual-mean wind. These conclusions are supported by the calculations based on the randomization of wind fluctuations (see blue lines in Fig. 10 for the trends as well as their statistical significance). Our study therefore highlights the large discrepancies between the widely-used reanalysis products regarding the relative contributions of the annual-mean wind and wind fluctuations to the observed changes of SO wind stress. These discrepancies may have contributed to the diverging responses of the SO simulated by ocean models forced with different reanalysis products (Gent 2016; Munday and Zhai 2017).

Figure 11 compares the trends of $\mathrm{MKE_{yr}}$, $\mathrm{EKE_{yr}}$, $\mathrm{EKE_{2d}}$, $\mathrm{EKE_{8d}}$ and $\mathrm{EKE_{2-8d}}$ in the three reanalysis products. All the trends shown in Fig. 11 are significant at <5% level, except for the trend of $\mathrm{EKE}_{2-8\mathrm{d}}$ in ERA-Interim (black line in Fig. 11f), which is not statistically significant. The trend of $\mathrm{EKE}_{\mathrm{yr}}$ in ERA-Interim (blue line in Fig. 11e), although significant, is much weaker than those in NCEP reanalysis products (blue lines in Figs. 11a and c). For example, the trends of $\mathrm{EKE}_{\mathrm{yr}}$ in NCEP R1 and NCEP R2 are over four times and nearly nine times greater than that in ERA-Interim, respectively. Furthermore, the trends of $\mathrm{EKE}_{\mathrm{yr}}$ (blue lines) are significantly greater than the trends of $\mathrm{MKE}_{\mathrm{yr}}$ (red lines) in both NCEP R1 and R2 (by 2.5 and 3.6 times, respectively; Figs. 11a and c), while the trend of $\mathrm{EKE}_{\mathrm{yr}}$ is less than half of the trend of $\mathrm{MKE}_{\mathrm{yr}}$ in ERA-Interim (Fig. 11e). The much weaker trend of $\mathrm{EKE}_{\mathrm{yr}}$ in ERA-Interim explains why wind fluctuations make little contribution to the observed increase of SO wind stress. Over 80% of the positive trends of $\mathrm{EKE}_{\mathrm{yr}}$ found in both NCEP R1 and R2 are accounted for by the trends of $\mathrm{EKE}_{8\mathrm{d}}$ (red lines in Figs. 11b and d vs blue lines in Figs. 11a and c). Both $\mathrm{EKE}_{2\mathrm{d}}$ and $\mathrm{EKE}_{2-8\mathrm{d}}$ contribute significantly to the increase of $\mathrm{EKE}_{8\mathrm{d}}$ (Figs. 11b and d). Our analysis thus shows that the SO has become stormier over the last four decades, and this increased storminess may have played an important role in the strengthening of SO wind stress, with ramifications for the sensitivity of SO stratification and circulation to wind stress changes (Munday and Zhai 2017).

The trends of the seasonal-mean SO wind stress are significant at <5% level in all four seasons in NCEP R1, with larger trends in austral summer and autumn (Fig. 12a). In comparison, the trends of the seasonal-mean wind stress in ERA-Interim (Fig. 12c) are much smaller and only significant in austral summer and autumn. The trends of the seasonal-mean EKE in NCEP R1 (Fig. 12b) are again found to be significant in all seasons, with larger values in austral summer and autumn, while no significant trend is found in ERA-Interim in any season (Fig. 12d). These results show that wind fluctuations in NCEP R1 contribute to the strengthening of not only the annual-mean wind stress but also the seasonal-mean wind stress in the SO. The greater contribution to the annual-mean trend by trends in austral summer and autumn is consistent with results from previous Antarctic radiosonde data and model studies, which showed that the trend of the SH circumpolar westerly is stronger during austral summer and autumn (Thompson and Solomon 2002; Fogt et al. 2009; Jones et al. 2016), as a result of the development of the Antarctic ozone depletion during the austral summer season (Gillett and Thompson 2003; Thompson et al. 2011).

4. Summary and Conclusions

The Southern Ocean plays a key role in regulating the global climate via its residual meridional overturning circulation and the Antarctic Circumpolar Current. It is therefore an important task to understand how the SO responds to the observed and predicted strengthening of the westerly wind stress. Recently, Munday and Zhai (2017) showed that the sensitivity of SO stratification and circulation to wind stress changes depends strongly on whether these changes in wind stress are brought about by changes of the mean wind or wind fluctuations. However, it is yet unknown whether wind fluctuations have played a role in shaping the observed wind stress changes in the SO. In this study, we have analyzed two widely-used atmospheric reanalysis products to assess the contribution of wind fluctuations to the mean, variability and trend of SO wind stress over the last four decades. Our main findings are:

- Wind fluctuations, particularly those associated with weather systems and baroclinic storms, significantly enhance the strength of the mean wind stress in the SO. The magnitude of peak zonal-mean wind stresses is found to be doubled when wind fluctuations are included in the stress calculation. Over 70% of this doubling effect is owing to fluctuations that last less than 8 days, i.e., associated primarily with weather systems/baroclinc storms.
- The SAM index is a good indicator for the mean westerly wind and wind stress, but is not as good a measure for wind fluctuations. Both the mean wind and mean wind stress are considerably stronger and also shifted poleward (by a few degrees) during positive SAM

years. In comparison, no significant differences in wind fluctuations are found between positive and negative SAM years. Therefore, stronger wind stresses during positive SAM years are due mainly to the stronger background mean winds, not enhanced wind variability, although the presence of wind fluctuations significantly amplifies wind stress differences between positive and negative SAM years.

- Large discrepancies are found between the reanalysis products analyzed in this study regarding the contribution of wind fluctuations to the strengthening trend of SO wind stress. The intensities of wind fluctuations in NCEP R1 and R2 have increased significantly over the last four decades and are found to contribute to about one-third and half of the increase in the strength of SO wind stress, respectively. In contrast, the intensity of wind fluctuations only experiences a very modest increase in ERA-Interim, and as such the wind stress trend in ERA-Interim is explained almost entirely by the strengthening of the mean westerly wind. Furthermore, the majority (over 80%) of the increase in wind fluctuations in NCEP R1 and R2 is found to be associated with weather systems and baroclinic storms. No significant trend is detected in JRA-55.
- The intensity of wind fluctuations exhibits a pronounced seasonal cycle, being highest in austral winter and lowest in austral summer. As a result, the peak zonal mean wind stress is greater in austral winter than in austral summer, despite the mean westerly wind being stronger in austral summer than austral winter. Furthermore, trends in austral summer and autumn are found to contribute most to the annual trend in the SO.

Results from this study highlight the important contributions of wind fluctuations, especially those associated with weather systems and baroclinic storms, to the mean, variability and trend of SO wind stress. Both NCEP and ERA-Interim reanalysis products show that the SO has become stormier over the last four decades, although the increase in atmospheric storminess is very modest in ERA-Interim. The large discrepancies found between reanalysis products regarding the contributions of wind fluctuations to the strengthening trend of SO wind stress are worrying, since not only the magnitude of the increased wind stress but also how this increase comes about matters for the SO response to changes in wind stress forcing (Munday and Zhai 2017). The discrepancies between reanalysis products also highlight the need to have sustained observations with better coverage in the SO in order to better understand the atmospheric forcing and its changes in a region that is vital for the global climate system.

Acknowledgments

This study is supported by the National Key R&D Program of China (2016YFA0601804). XL is supported by a scholarship from the Chinese Scholarship Council and by the National Natural Science Foundation of China (41406214). XZ acknowledges additional support from the School of Environmental Sciences, University of East Anglia. ZW is supported by the Fundamental Research Funds for the Central Universities (2017B04814, 2017B20714). DRM is supported by the Natural Environment Research Council (ORCHESTRA, grant number NE/N018095/1). We wish to thank Clothilde Langlais and two anonymous reviewers for their constructive comments that led to an improved manuscript.

References

Bishop, S. P., P. R. Gent, F. O. Bryan, A. F. Thompson, M. C. Long, and R. Abernathey, 2016: Southern Ocean Overturning Compensation in an Eddy-Resolving Climate Simulation. *J. Phys. Oceanogr.*, **46**(5), 1575–1592.

Böning, C. W., A. Dispert, M. Visbeck, S. R. Rintoul, and F. U. Schwarzkopf, 2008: The response of the Antarctic Circumpolar Current to recent climate change. *Nat. Geosci.*, **1**, 864–869, doi:10.1038/ngeo362.

Chang, E. K. M., 2017: Projected Significant Increase in the Number of Extreme Extratropical

Cyclones in the Southern Hemisphere. *J. Climate*, **30**, 4915–4935.
Dee, D. P., and Coauthors, 2011: The ERA-Interim reanalysis: configuration and performance of the data assimilation system. *Quart. J. Roy. Meteor. Soc.*, **137**, 553–597.
Downes, S.M., A. S. Budnick, J. L. Sarmiento, and R. Farneti, 2011: Impacts of wind stress on the Antarctic Circumpolar Current fronts and associated subduction. *Geophys. Res. Lett.*, **38**, L11605doi:10.1029/2011GL047668.
Dufour, C. O., J. Le Sommer, J. D. Zika, M. Gehlen, J. C. Orr, P. Mathiot, and B. Barnier, 2012: Standing and transient eddies in the response of the Southern Ocean meridional overturning to the southern annular mode. *J. Climate*, **25**, 6958–6974, doi:10.1175/JCLI-D-11-00309.1.
Farneti, R., T. L. Delworth, A. J. Rosati, S. M. Griffies, and F. Zeng, 2010: The role of mesoscale eddies in the rectification of the Southern Ocean response to climate change. *J. Phys. Oceanogr.*, **40**, 1539–1557, doi:10.1175/2010JPO4353.1.
Fogt, R. L., and Coauthors, 2009: Historical SAM variability. Part II: Twentieth-century variability and trends from reconstructions, observations, and the IPCC AR4 Models. *J. Climate*, **22**, 5346–5365.
Franzke, C., T. J. O'kane, D. Monselesan, J. Risbey, and I. Horenko, 2015: Systematic attribution of observed Southern Hemispheric circulation trends to external forcing and internal variability. *Nonlin. Processes Geophys.*, **22**, 513–525, doi:10.5194/npgd-2-675-2015.
Gent, P., 2016: Effects of southern hemisphere wind changes on the meridional overturning circulation in models. *Ann. Rev. Mar. Sci.*, **8**, 79–94.
Gillett, N. P., and D. W. J. Thompson, 2003: Simulation of recent Southern Hemisphere climate change. *Science*, **302**, 273–275, doi:10.1126/science.1087440.

Gong, D., and S. Wang, 1999: Definition of Antarctic oscillation index. *Geophys. Res. Lett.*, **26**, 459–462.

Grieger, J., G. C. Leckebusch, M. G. Donat, M. Schuster, and U. Ulbrich, 2014: Southern Hemisphere winter cyclone activity under recent and future climate conditions in multi model AOGCM simulations. *Int. J. Climatol.*, **34**, 3400–3416.

Hallberg, R., and A. Gnanadesikan, 2001: An exploration of the role of transient eddies in determining the transport of a zonally reentrant current. *J. Phys. Oceanogr.*, **31**, 3312–3330.

——, and A. Gnanadesikan, 2006: The role of eddies in determining the structure and response of the wind-driven southern hemisphere overturning: Results from the Modeling Eddies in the Southern Ocean (MESO) project. *J. Phys. Oceanogr.*, **36**, 2232–2252.

Hines, K. M., D. H. Bromwich, and G. J. Marshall, 2000: Artificial surface pressure trends in the NCEP–NCAR reanalysis over the Southern Ocean and Antarctica. *J. Climate*, **13**, 3940–3952.

Hogg, A. M., P. Spence, O.A. Saenko, and S.M. Downes, 2017: The Energetics of Southern Ocean Upwelling. *J. Phys. Oceanogr.*, **47**, 135–153, https://doi.org/10.1175/JPO-D-16-0176.1.

Inatsu, M., and B. J. Hoskins, 2004: The zonal asymmetry of the Southern Hemisphere winter storm track. *J. Climate*, **17**(24), 4882-4892.

Jones, J. M., and Coauthors, 2016: Assessing recent trends in high-latitude Southern Hemisphere surface climate. *Nat. Clim. Change*, **6**(10), 917–926.

Jouanno, J., X. Capet, G. Madec, G. Roullet, and P. Klein, 2016: Dissipation of the energy imparted by mid-latitude storms in the Southern Ocean. *Ocean Sci.*, **12**, 743–769.

Jung, T., S. K. Gulev, I. Rudeva, and V. Soloviov, 2006: Sensitivity of extratropical cyclones characteristics to horizontal resolution in the ECMWF model. *Q. J. R. Meteorol. Soc.*,

132, 1839–1857, doi:10.1256/qj.05.212.

Kalnay, E., and Coauthors, 1996: The NCEP/NCAR 40-Year Reanalysis Project. *Bull. Amer. Meteor. Soc.*, **77**, 437–471.

Kanamitsu, M., W. Ebisuzaki, J. Woollen, S.-K. Yang, J. J. Hnilo, M. Fiorino, and G. L. Potter, 2002: NCEP–DOE AMIP-II Reanalysis (R-2). *Bull. Amer. Meteorol. Soc.*, **83**, 1631–1643.

Kobayashi, S., Y. Ota, Y. Harada, et al., 2015: The JRA-55 reanalysis: General specifications and basic characteristics. *J. Meteor. Soc. Japan.*, **93**(1), 5–48.

Langlais, C., S. Rintoul, J. Zika, 2015: Sensitivity of Antarctic circumpolar transport and eddy activity to wind patterns in the Southern Ocean. *J. Phys. Oceanogr.*, **45**, 1051–1067. doi:10.1175/JPO-D-14-0053.1.

Large, W. G., J. C. McWilliams, and S. C. Doney, 1994: Oceanic vertical mixing: A review and a model with a nonlocal boundary layer parameterization. *Rev. Geophys.*, **32**, 363–403.

Le Quéré, C., and Coauthors, 2008: Saturation of the Southern Ocean CO2 sink due to recent climate change. *Science*, **316**(5831), 1735–1738.

Marshall, G. J., 2003: Trends in the Southern Annular Mode from observations and reanalyses. *J. Climate*, **16**, 4134–4143.

Marshall, J., and K. Speer, 2012: Closure of the meridional overturning circulation through Southern Ocean upwelling. *Nat. Geosci.*, **5**(3), 171–180.

Meredith, M. P., and A. M. Hogg, 2006: Circumpolar response of Southern Ocean eddy activity to a change in the southern annular mode. *Geophys. Res. Lett.*, **33**, L16608, doi:10.1029/2006GL026499.

Munday, D. R., H. L. Johnson, and D. P. Marshall, 2013: Eddy saturation of equilibrated circumpolar currents. *J. Phys. Oceanogr.*, **43**, 507–532.

——, and X. Zhai, 2015: Sensitivity of Southern Ocean circulation to wind stress changes: role of relative wind stress. *Ocean Modell.*, **95**, 15–24.

——, and ——, 2017: The Impact of Atmospheric Storminess on the Sensitivity of Southern Ocean Circulation to Wind Stress Changes. *Ocean Modell.*, **115**, 14–26.

O'Kane, T. J., R. J. Matear, M. A. Chamberlain, J. S. Risbey, B. M. Sloyan, and I. Horenko, 2013: Decadal variability in an OGCM Southern Ocean: Intrinsic modes, forced modes and metastable states. *Ocean Modell.*, **69**, 1–21.

Screen, J. A., N. P. Gillett, D. P. Stevens, G. J. Marshall, and H. K. Roscoe, 2009: The role of eddies in the Southern Ocean temperature response to the southern annular mode. *J. Climate*, **22**, 806–818, doi:10.1175/2008JCLI2416.1.

Simmonds, I., and K. Keay, 2000: Mean Southern Hemisphere extratropical cyclone behavior in the 40-year NCEP–NCAR reanalysis. *J. Climate*, **13**(5), 873–885.

Sinha, A. and R. P. Abernathey, 2016: Time scale of Southern Ocean eddy equilibration. *J. Phys. Oceanogr.*, **46**, 2785–2805, doi:10.1175/JPO–D–16–0041.1.

Spence, P., S. M. Griffies, M. H. England, A. M. Hogg, O. A. Saenko, and N. C. Jourdain, 2014: Rapid subsurface warming and circulation changes of Antarctic coastal waters by poleward shifting winds. *Geophys. Res. Lett.*, **41**(13), 4601–4610, doi:10.1002/2014GL060613, 2014GL060613.

Straub, D. N., 1993: On the transport and angular momentum balance of channel models of the Antarctic Circumpolar Current. *J. Phys. Oceanogr.*, **23**, 776-782.

Swart, N. C., and J. C. Fyfe, 2012: Observed and simulated changes in the Southern Hemisphere surface westerly wind-stress. *Geophys. Res. Lett.*, **39**, L16711, doi:10.1029/2012GL052810.

Thompson, D. W. J., and S. Solomon, 2002: Interpretation of recent Southern Hemisphere climate change. *Science*, **296**(5569), 895–899.

——, ——, P. J. Kushner, M. H. England, K. M. Grise, and D. J. Karoly, 2011: Signatures of the Antarctic ozone hole in Southern Hemisphere surface climate change. *Nat. Geosci.*, **4**, 741–749, doi:10.1038/ngeo1296.

Thomas, J. L., D. W. Waugh, and A. Gnanadesikan, 2015: Southern Hemisphere extratropical circulation: Recent trends and natural variability. *Geophys. Res. Lett.*, **42**, doi:10.1002/2015GL064521.

Tilinina, N., S. K. Gulev, I. Rudeva, and P. Koltermann, 2013: Comparing cyclone life cycle characteristics and their interannual variability in different reanalyses. *J. Climate*, **26**, 6419–6438.

Trenberth, K. E., 1991: Storm tracks in the Southern Hemisphere. *J. Atmospheric Sci.*, **48**(19), 2159–2178.

Turner, J., and co-authors, 2004: The SCAR READER project: Towards a high-quality database of mean Antarctic meteorological observations. *J. Clim*ate, 17, 2890–2898.

Verezemskaya, P., N. Tilinina, S. Gulev, I. A. Renfrew, and M. Lazzara, 2017: Southern Ocean mesocyclones and polar lows from manually tracked satellite mosaics. *Geophys. Res. Lett.*, **44**(15), 7985–7993.

Viebahn, J., and C. Eden, 2010: Towards the impact of eddies on the response of the Southern Ocean to climate change. *Ocean Modell.*, **34**(3), 150–165.

Wang, X. L., Y. Feng, R. Chan, and V. Isaac, 2016: Inter-comparison of extra-tropical cyclone activity in nine reanalysis datasets. *Atmos. Res.*, **181**, 133–153.

Wang, Z., X. Zhang, Z. Guan, B. Sun, X. Yang, and C. Liu, 2015: An atmospheric origin of the multi-decadal bipolar seesaw. *Scientific Reports*, **5**, 8909.

Wang, Z., Y. Wu, X. Lin, C. Liu, Z. Xie, 2017: Impacts of open-ocean deep convection in the Weddell Sea on coastal and bottom water temperature. *Climate Dyn.*, **48**: 2967-2981, doi:10.1007/s00382-016-3244-y.

Wu, Y., X. Zhai, and Z. Wang, 2016: Impact of synoptic atmospheric forcing on the mean ocean circulation. *J. Climate*, **29**(16), 5709–5724.

——, ——, and ——, 2017: Decadal-mean impact of including ocean surface currents in bulk formula on surface air-sea fluxes and ocean general circulation. *J. Climate*, doi:10.1175/JCLI-D-17-0001.

Yin, J. H., 2005: A consistent poleward shift of the storm tracks in simulations of 21st century climate. *Geophys. Res. Lett.*, **32**, L18701.

Zappa, G., L. Shaffrey, and K. I. Hodges, 2014: Can polar lows be objectively identified and tracked in the ECMWF operational analysis and the ERA-Interim reanalysis? *Mon. Weather Rev.*, **142**(8), 2596–2608.

Zhai, X., 2013: On the wind mechanical forcing of the ocean general circulation. *J. Geophys. Res. Oceans*, **118**(12), 6561–6577.

——, and C. Wunsch, 2013: On the variability of wind power input to the oceans with a focus on the subpolar North Atlantic. *J. Climate*, **26**(11), 3892–3903.

——, and D. R. Munday, 2014: Sensitivity of Southern Ocean overturning to wind stress changes: Role of surface restoring time scales. *Ocean Modell.*, **84**, 12–25.

——, H. L. Johnson, D. P. Marshall, and C. Wunsch, 2012: On the wind power input to the ocean general circulation. *J. Phys. Oceanogr.*, **42**, 1357–1365.

Zhou, S., X. Zhai, and I. A. Renfrew, 2018: The impact of high-frequency weather systems on SST and surface mixed layer in the central Arabian Sea. *J. Geophys. Res.*, 123, doi:10.1002/2017JC013609.

List of Table

1. List of variables and the formulas used to calculate them. Overbars "$\overline{}^{\mathrm{yr}}$", "$\overline{}^{\mathrm{2d}}$", "$\overline{}^{\mathrm{8d}}$" and "$\overline{}^{\mathrm{2-8d}}$" represent annual mean, 2-day running mean, 8-day running mean, and 2-8 day filtered, respectively, and superscript "6hr" indicates 6-hourly reanalysis winds. The 2-8 day filtered winds ($\overline{\mathrm{u}_{10}}^{2-8\mathrm{d}}$ and $\overline{\mathrm{v}_{10}}^{2-8\mathrm{d}}$) are obtained by removing winds fluctuations on time scales of 2 to 8 days from the origional 6-hourly reanalysis wind field, and are calculated using $\overline{\mathrm{u}_{10}}^{2-8\mathrm{d}} = \mathrm{u}_{10}^{6\mathrm{hr}} - (\overline{\mathrm{u}_{10}}^{2\mathrm{d}} - \overline{\mathrm{u}_{10}}^{8\mathrm{d}})$ and $\overline{\mathrm{v}_{10}}^{2-8\mathrm{d}} = \mathrm{v}_{10}^{6\mathrm{hr}} - (\overline{\mathrm{v}_{10}}^{2\mathrm{d}} - \overline{\mathrm{v}_{10}}^{8\mathrm{d}})$, respectively. The 2-8 day filtered wind speed ($\left|\overline{\mathrm{U}_{10}}^{2-8\mathrm{d}}\right|$) is then calculated from $\left|\overline{\mathrm{U}_{10}}^{2-8\mathrm{d}}\right| = \sqrt{(\overline{\mathrm{u}_{10}}^{2-8\mathrm{d}})^2 + (\overline{\mathrm{v}_{10}}^{2-8\mathrm{d}})^2}$.

Table 1. List of variables and the formulas used to calculate them. Overbars "$\overline{\ \ }^{yr}$", "$\overline{\ \ }^{2d}$", "$\overline{\ \ }^{8d}$" and "$\overline{\ \ }^{2-8d}$" represent annual mean, 2-day running mean, 8-day running mean, and 2-8 day filtered, respectively, and superscript "6hr" indicates 6-hourly reanalysis winds. The 2-8 day filtered winds ($\overline{u_{10}}^{2-8d}$ and $\overline{v_{10}}^{2-8d}$) are obtained by removing winds fluctuations on time scales of 2 to 8 days from the origional 6-hourly reanalysis wind field, and are calculated using $\overline{u_{10}}^{2-8d} = u_{10}^{6hr} - (\overline{u_{10}}^{2d} - \overline{u_{10}}^{8d})$ and $\overline{v_{10}}^{2-8d} = v_{10}^{6hr} - (\overline{v_{10}}^{2d} - \overline{v_{10}}^{8d})$, respectively. The 2-8 day filtered wind speed ($\left|\overline{U_{10}}^{2-8d}\right|$) is then calculated from $\left|\overline{U_{10}}^{2-8d}\right| = \sqrt{(\overline{u_{10}}^{2-8d})^2 + (\overline{v_{10}}^{2-8d})^2}$.

Variable	Defination	Formula
$\boldsymbol{\tau_{6hr}}$	Zonal wind stress calculated from 6-hourly winds	$\overline{\rho_a c_d \left\|U_{10}^{6hr}\right\| u_{10}^{6hr}}^{yr}$
$\boldsymbol{\tau_{2d}}$	Zonal wind stress calcuated from 2-day running mean winds	$\overline{\rho_a c_d \left\|\overline{U_{10}}^{2d}\right\| \overline{u_{10}}^{2d}}^{yr}$
$\boldsymbol{\tau_{8d}}$	Zonal wind stress calcuated from 8-day running mean winds	$\overline{\rho_a c_d \left\|\overline{U_{10}}^{8d}\right\| \overline{u_{10}}^{8d}}^{yr}$
$\boldsymbol{\tau_{2-8d}}$	Zonal wind stress calcuated from 2-8 day filtered winds	$\overline{\rho_a c_d \left\|\overline{U_{10}}^{2-8d}\right\| \overline{u_{10}}^{2-8d}}^{yr}$
$\boldsymbol{\tau_{yr}}$	Zonal wind stress calculated from annual-mean winds	$\overline{\rho_a c_d \left\|\overline{U_{10}}^{yr}\right\| \overline{u_{10}}^{yr}}^{yr}$
$\mathbf{MKE_{yr}}$	Kinetic energy associated with annual-mean winds	$\dfrac{\overline{(\overline{u_{10}}^{yr})^2 + (\overline{v_{10}}^{yr})^2}^{yr}}{2}$
$\mathbf{EKE_{yr}}$	Kinetic energy associated with wind fluctuations on time scales of	$\dfrac{\overline{(u_{10}^{6hr} - \overline{u_{10}}^{yr})^2 + (v_{10}^{6hr} - \overline{v_{10}}^{yr})^2}^{yr}}{2}$

	6 hours to 1 year	
$\mathbf{EKE_{2d}}$	Kinetic energy calculated from wind fluctuations on time scales of 6 hours to 2 days alone	$\frac{\overline{(u_{10}^{6hr}-\overline{u_{10}}^{2d})^2+(v_{10}^{6hr}-\overline{v_{10}}^{2d})^2}^{yr}}{2}$
$\mathbf{EKE_{8d}}$	Kinetic energy calculated from wind fluctuations on time scales of 6 hours to 8 days alone	$\frac{\overline{(u_{10}^{6hr}-\overline{u_{10}}^{8d})^2+(v_{10}^{6hr}-\overline{v_{10}}^{8d})^2}^{yr}}{2}$
$\mathbf{EKE_{2-8d}}$	Kinetic energy calculated from wind fluctuations on time scales of 2 days to 8 days alone	$\frac{\overline{(\overline{u_{10}}^{2d}-\overline{u_{10}}^{8d})^2+(\overline{v_{10}}^{2d}-\overline{v_{10}}^{8d})^2}^{yr}}{2}$

List of Figures

7. The 1979-2016 station-based SAM index from Marshall (2003; updated online). Years with SAM>0.5 are defined here as positive SAM years and those with SAM<-0.5 negative SAM years.

8. The mean τ_{6hr} (N m^{-2}), MKE_{yr} and EKE_{yr} (m^{2} s^{-2}) averaged over positive and negative SAM years during 1979-2016 from NCEP R1 (a-h) and ERA-Interim (i-p). (b) and (j) are the mean stresses calculated using a combination of the mean wind averaged over all the positive SAM years and wind fluctuations from each negative SAM year. (f) and (n) are the mean stresses calculated using a combination of the mean wind averaged over all the negative SAM years and wind fluctuations from each positive SAM year.

9. Zonal-mean τ_{6hr} (N m^{-2}, a and d), MKE_{yr} (m^{2} s^{-2}, b and e), and EKE_{yr} (m^{2} s^{-2}, c and f) averaged over positive (solid black lines) and negative (dashed black lines) SAM years during 1979-2016 from NCEP R1 (a-c) and ERA-Interim (d-f). The grey lines mark one standard deviation.

10. Time series (red solid) and trend (red dashed) of SO wind stress averaged between 35^{o}S and 65^{o}S during 1979-2016 from (a) NCEP R1, (b) NCEP R2 and (c) ERA-Interim. Black lines are for wind stress obtained by randomizing the annual-mean winds and blue lines for that obtained by randomizing wind fluctuations. Percentages in brackets show statistical significance of the trends. Note that although the overall wind stress trends are positive when averaged between 35^{o}S and 65^{o}S, there are regions of negative trends, particularly between 35^{o}S and 45^{o}S (not shown).

11. Time series (solid) and trends (dashed) of MKE_{yr}, EKE_{yr}, EKE_{8d}, EKE_{2d} and EKE_{2-8d} (m^{2} s^{-2}) averaged between 35^{o}S and 65^{o}S during 1979-2016 from NCEP R1 (a-b), NCEP R2 (c-d) and ERA-Interim (e-f). Percentages in brackets show statistical significance of the trends.

12. Time series (solid) and trends (dashed) of the seasonal-mean τ_{6hr} (N m^{-2}, a and c) and EKE_{yr} (m^{2} s^{-2}, b and d) averaged between 35^{o}S and 65^{o}S during 1979-2016 from NCEP R1 (a-

b) and ERA-Interim (c-d). Percentages in brackets show statistical significance of the trends.

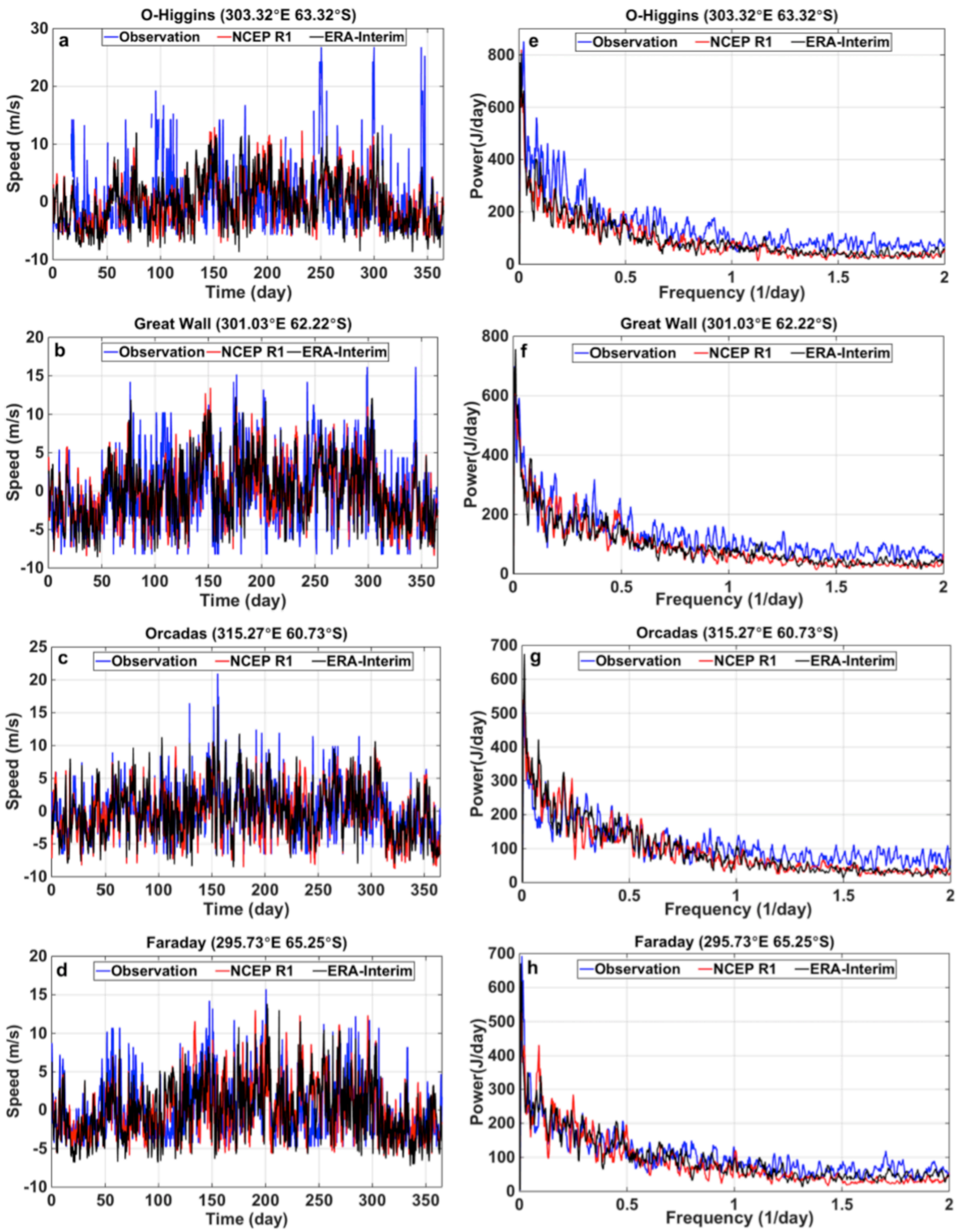

FIG. 1. Comparison of the time series and power spectra of 10-m wind speeds from NCEP R1 and ERA-Interim with automatic weather station data at four locations in 1989 (with the annual mean removed). The wind speeds are observed at 10 m, 10 m, 6 m and 11 m at O-Higgins, Great Wall, Orcadas and Faraday, respectively.

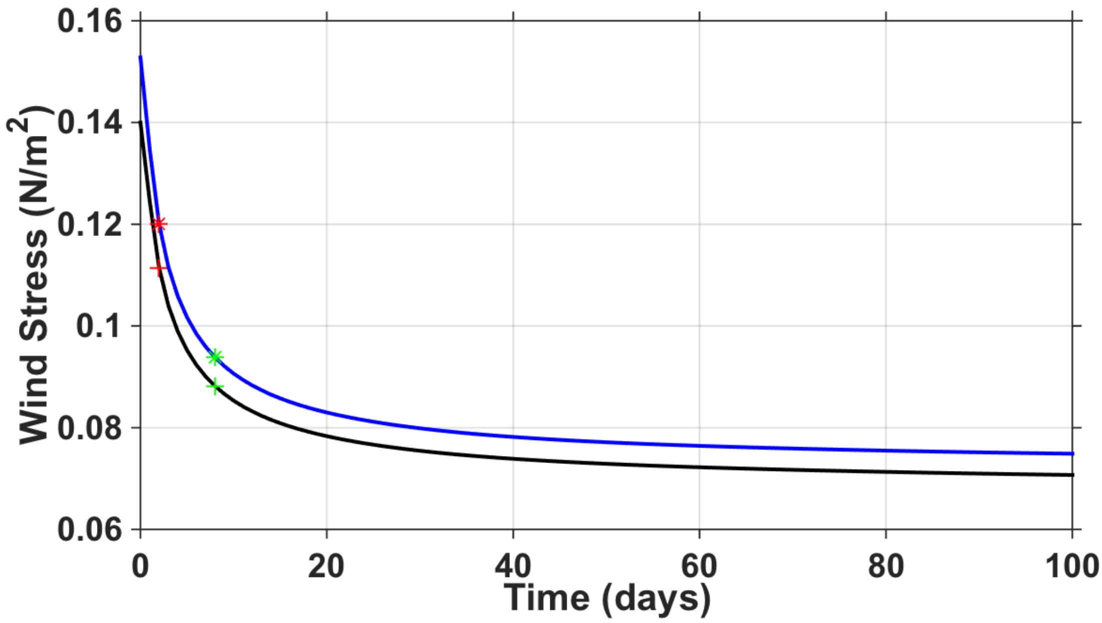

FIG. 2. The magnitude of peak zonal-mean zonal wind stress in the Southern Ocean ([35^{o}S 65^{o}S]) averaged over 1979-2016 as a function of the running mean time scale from NCEP R1 (black line) and ERA-Interim (blue line). Red and green crosses (stars) mark peak zonal-mean zonal wind stresses calculated from NCEP R1 (ERA-Interim) 2-day and 8-day running mean winds, respectively.

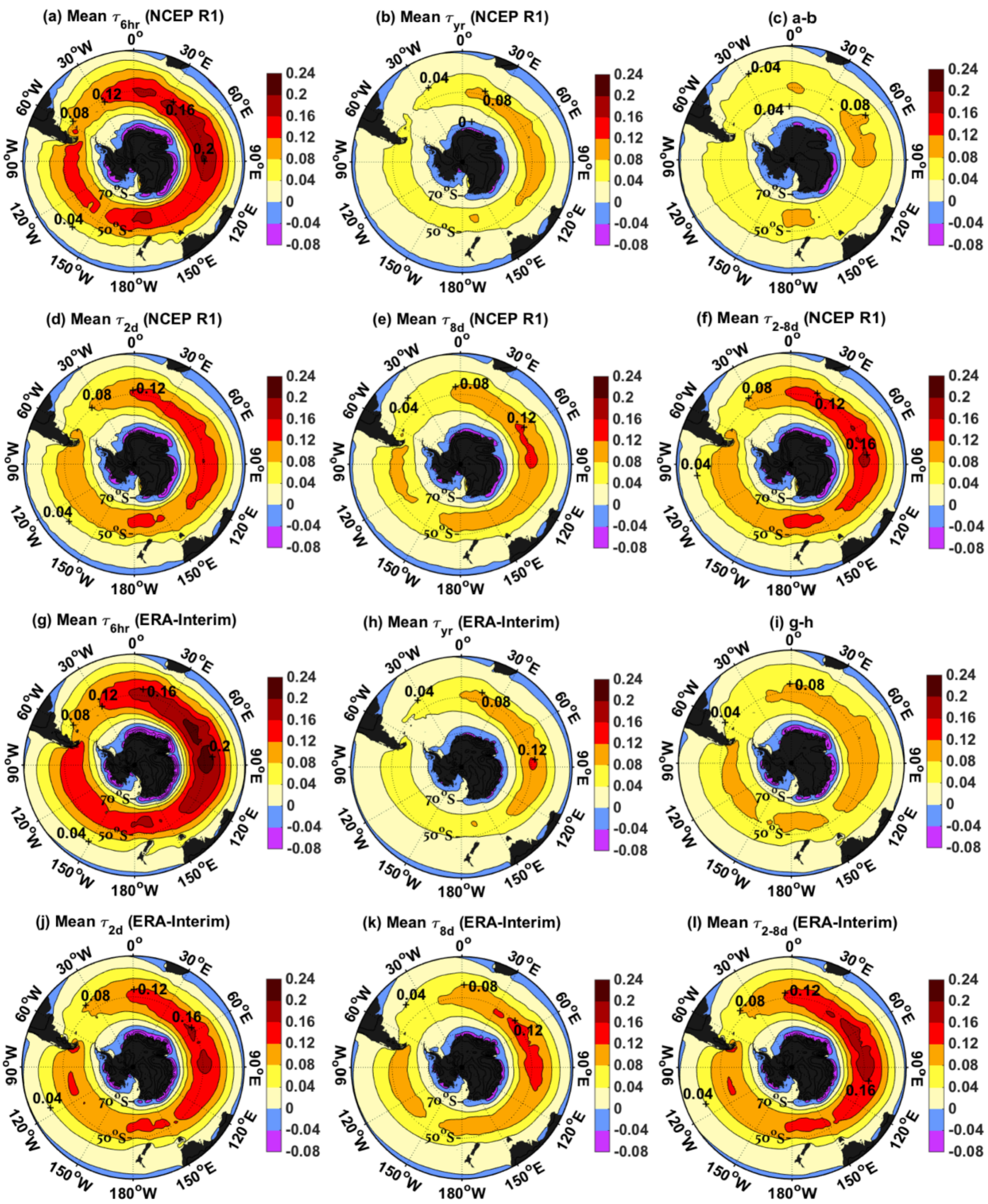

FIG. 3. The 1979-2016 time-mean wind stress (N m^{-2}) in the SO from NCEP R1 (a-f) and ERA-Interim (g-l). Mean τ_{6hr}, τ_{2d}, τ_{8d}, τ_{2-8d} and τ_{yr} are calculated from 6-hourly, 2-day running mean, 8-day running mean, 2-8 day filtered, and annual-mean winds, respectively (see Table 1). (c) and (i) are differences between τ_{6hr} and τ_{yr}, i.e. (a)-(b) and (g)-(h), respectively.

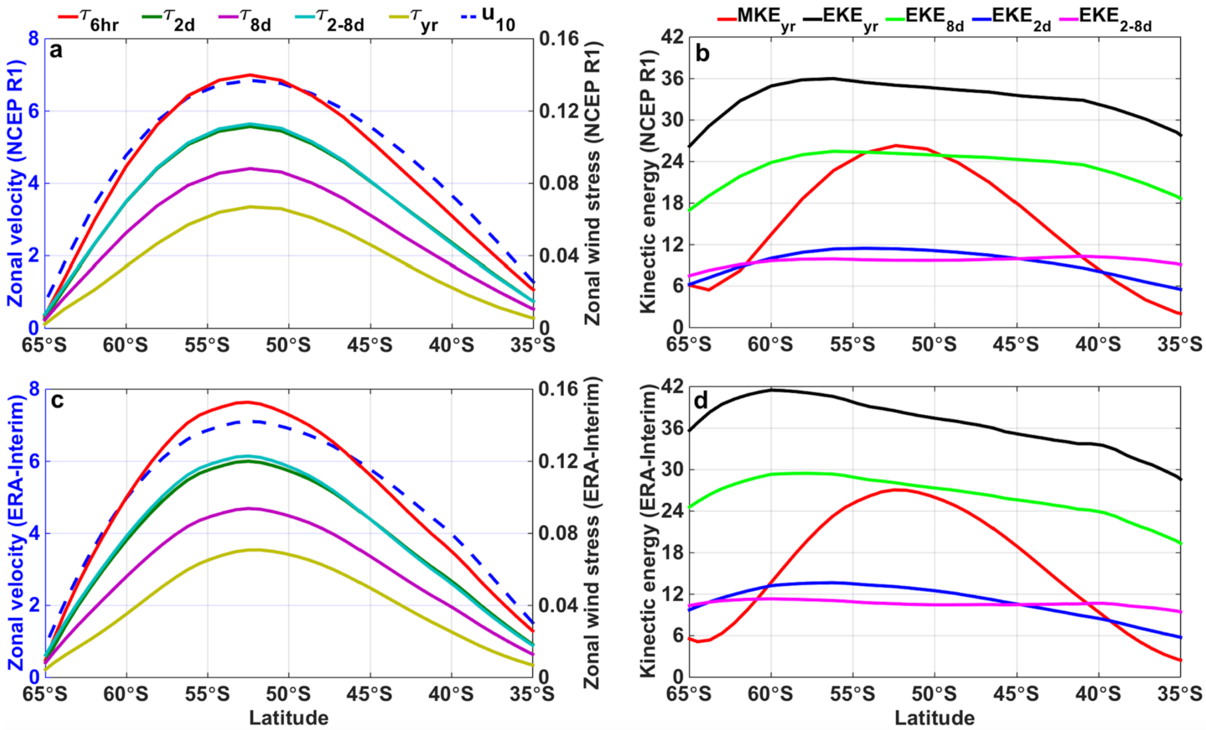

FIG. 4. The 1979-2016 zonal-mean and time-mean zonal wind velocity (dashed; m s^{-1}), zonal wind stresses (solid; N m^{-2}), mean and eddy kinetic energy (m^2 s^{-2}) from NCEP R1 (a-b) and ERA-Interim (c-d). MKE_{yr} is kinetic energy associated with the annual-mean winds, and EKE_{2d}, EKE_{2-8d}, EKE_{8d} and EKE_{yr} are kinetic energy calculated from wind fluctuations on time scales of 6 hours to 2 days, 2 to 8 days, 6 hours to 8 days, and 6 hours to 1 year, respectively (see Table 1).

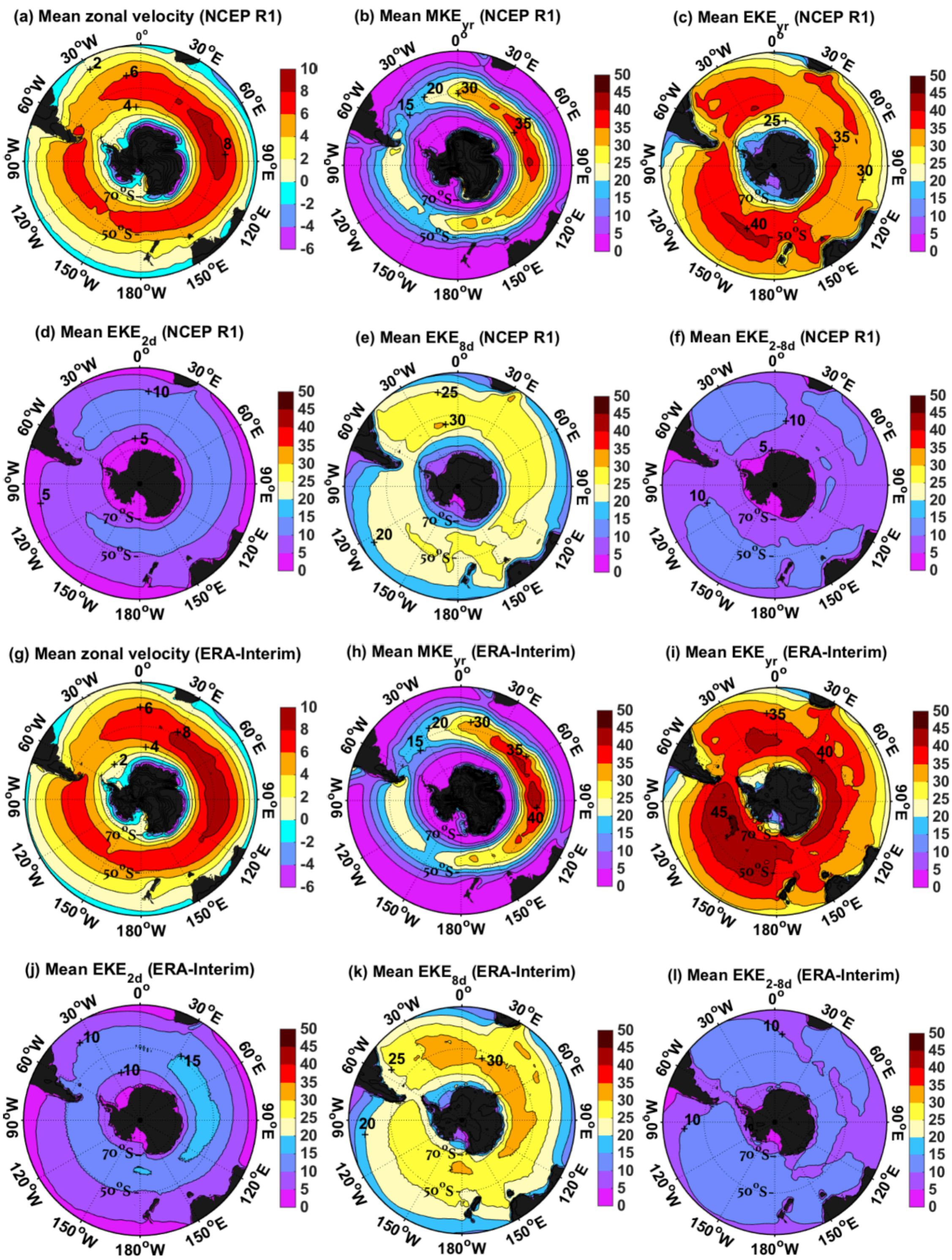

FIG. 5. The 1979-2016 time-mean zonal wind velocity (m s^{-1}), mean kinetic energy (m^2 s^{-2}) and eddy kinetic energy (m^2 s^{-2}) in the SO from NCEP R1 (a-f) and ERA-Interim (g-l).

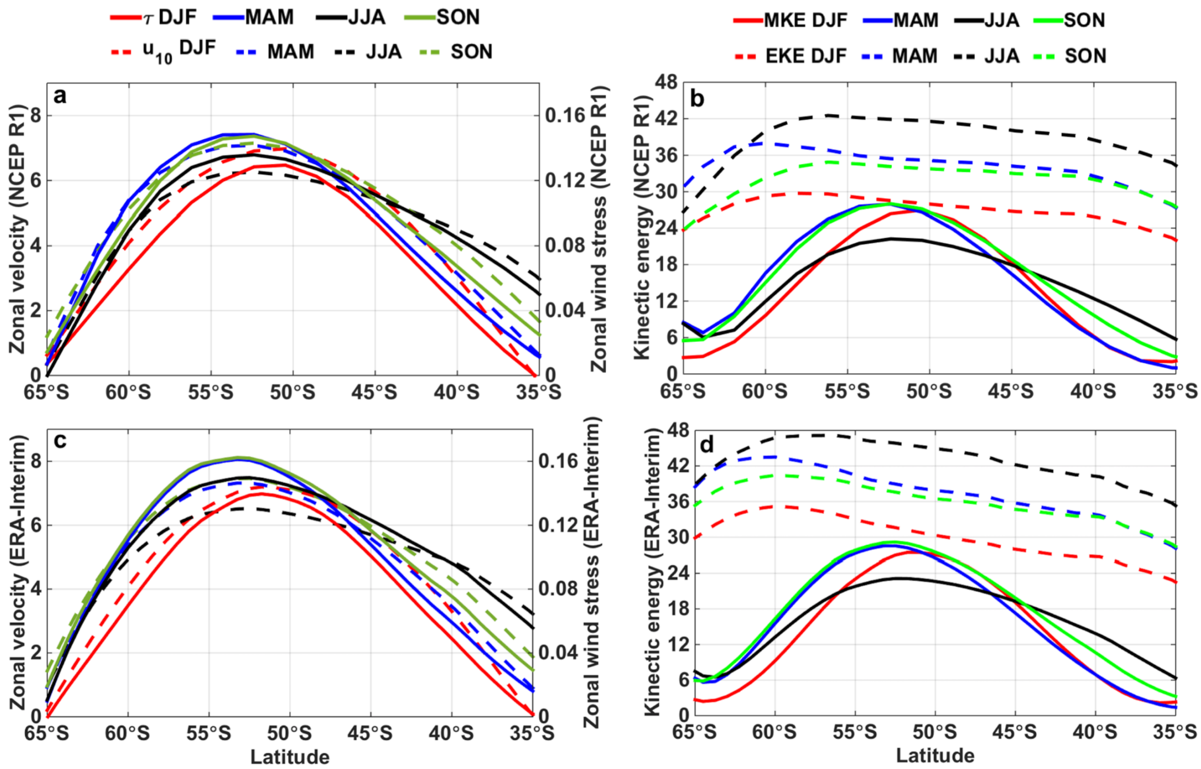

FIG. 6. The 1979-2016 zonal-mean and seasonal-mean zonal wind velocity (dashed; m s^{-1}), zonal wind stress (solid; N m^{-2}), mean kinetic energy (solid; m^2 s^{-2}) and eddy kinetic energy (dashed; m^2 s^{-2}) from NCEP R1 (a-b) and ERA-Interim (c-d).

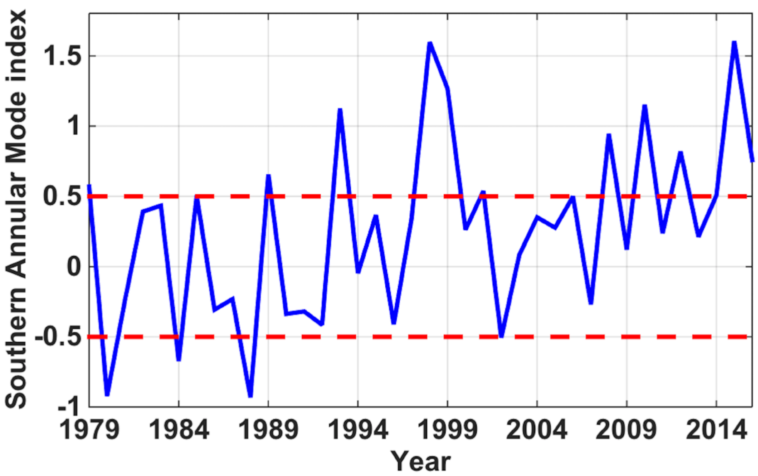

FIG. 7. The 1979-2016 station-based SAM index from Marshall (2003; updated online). Years with SAM>0.5 are defined here as positive SAM years and those with SAM<-0.5 negative SAM years.

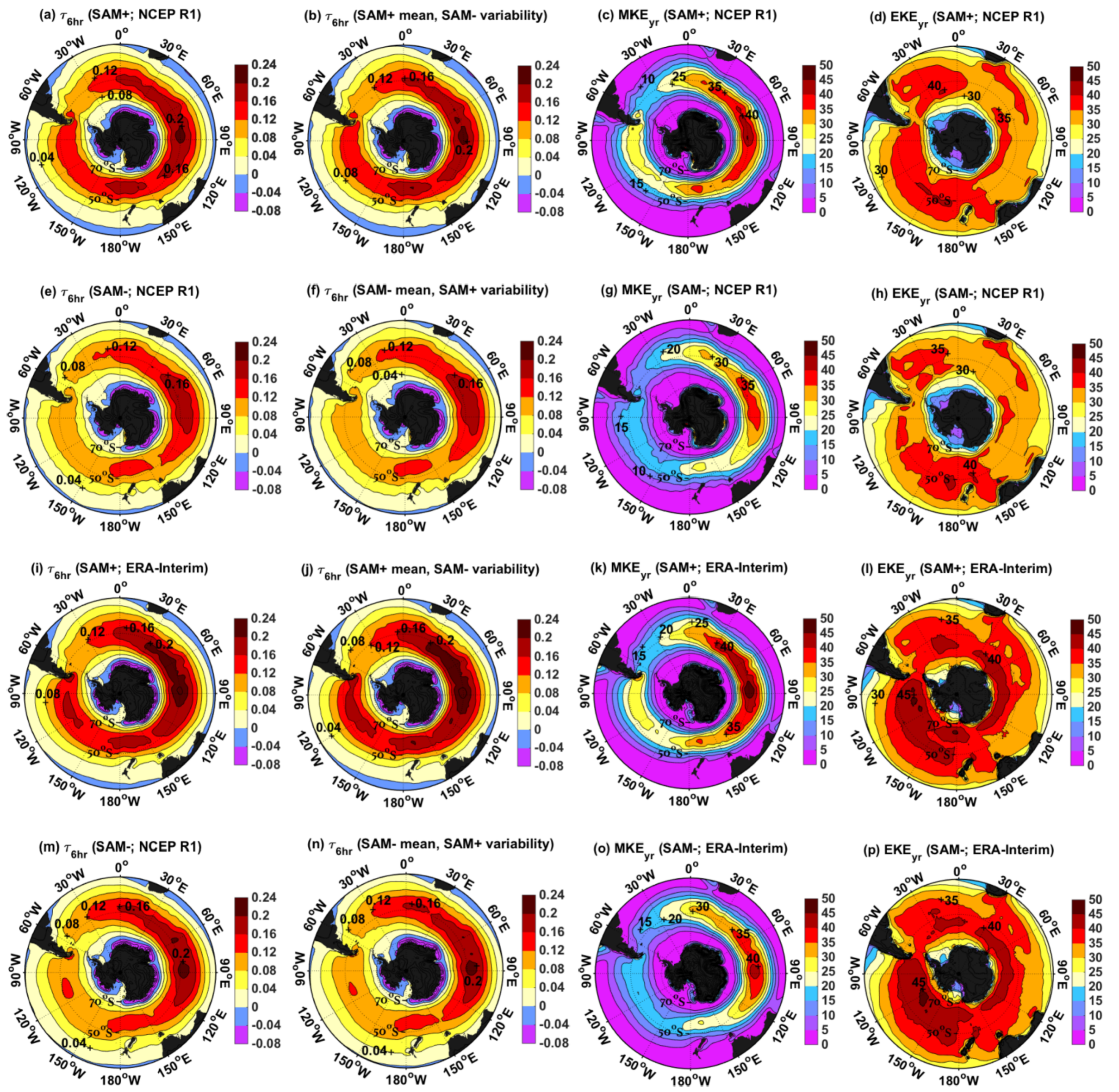

FIG. 8. The mean τ_{6hr} (N m^{-2}), MKE$_{yr}$ and EKE$_{yr}$ (m^2 s^{-2}) averaged over positive and negative SAM years during 1979-2016 from NCEP R1 (a-h) and ERA-Interim (i-p). (b) and (j) are the mean stresses calculated using a combination of the mean wind averaged over all the positive SAM years and wind fluctuations from each negative SAM year. (f) and (n) are the mean stresses calculated using a combination of the mean wind averaged over all the negative SAM years and wind fluctuations from each positive SAM year.

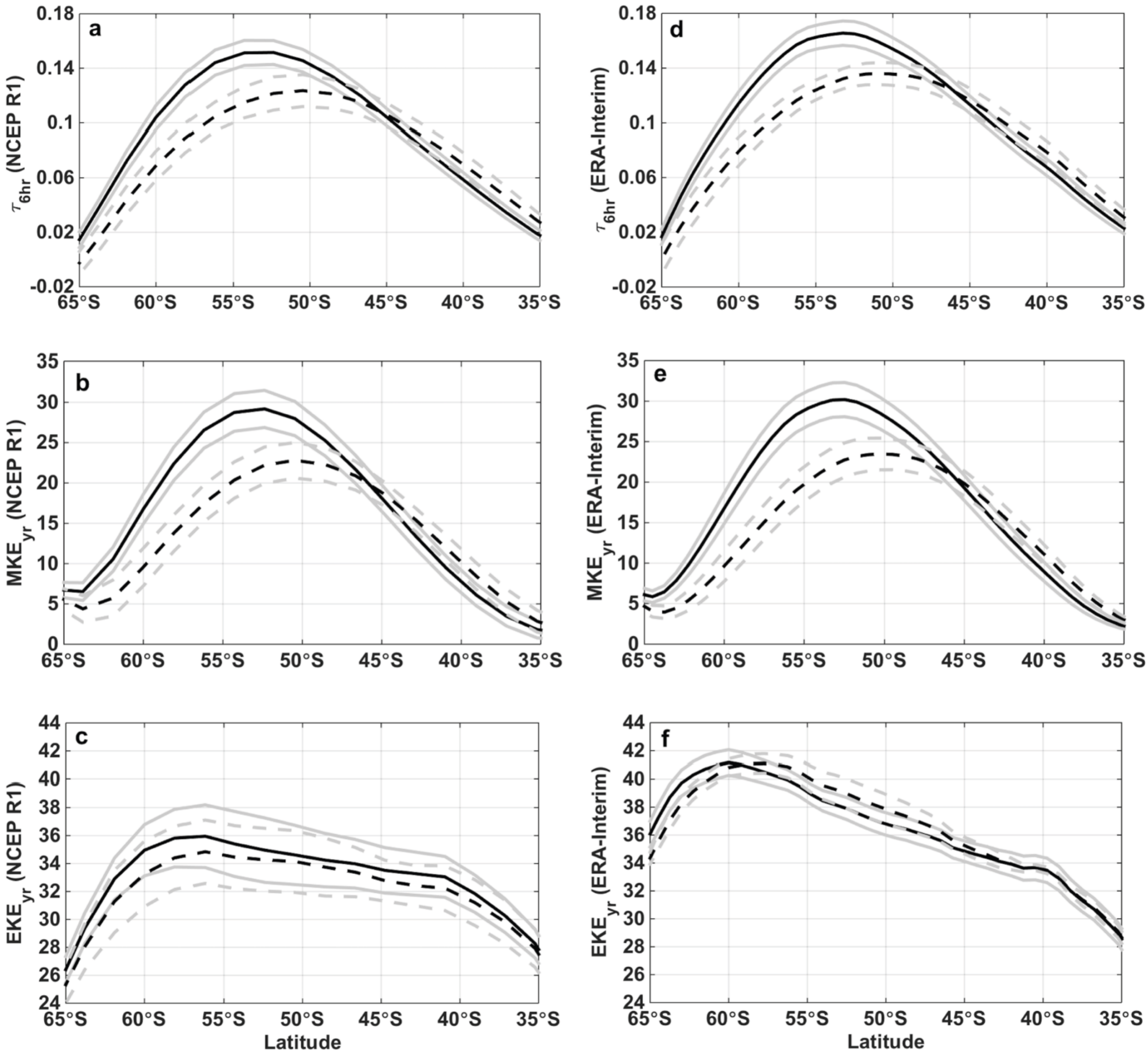

FIG. 9. Zonal-mean τ_{6hr} (N m^{-2}, a and d), MKE_{yr} (m^2 s^{-2}, b and e), and EKE_{yr} (m^2 s^{-2}, c and f) averaged over positive (solid black lines) and negative (dashed black lines) SAM years during 1979-2016 from NCEP R1 (a-c) and ERA-Interim (d-f). The grey lines mark one standard deviation.

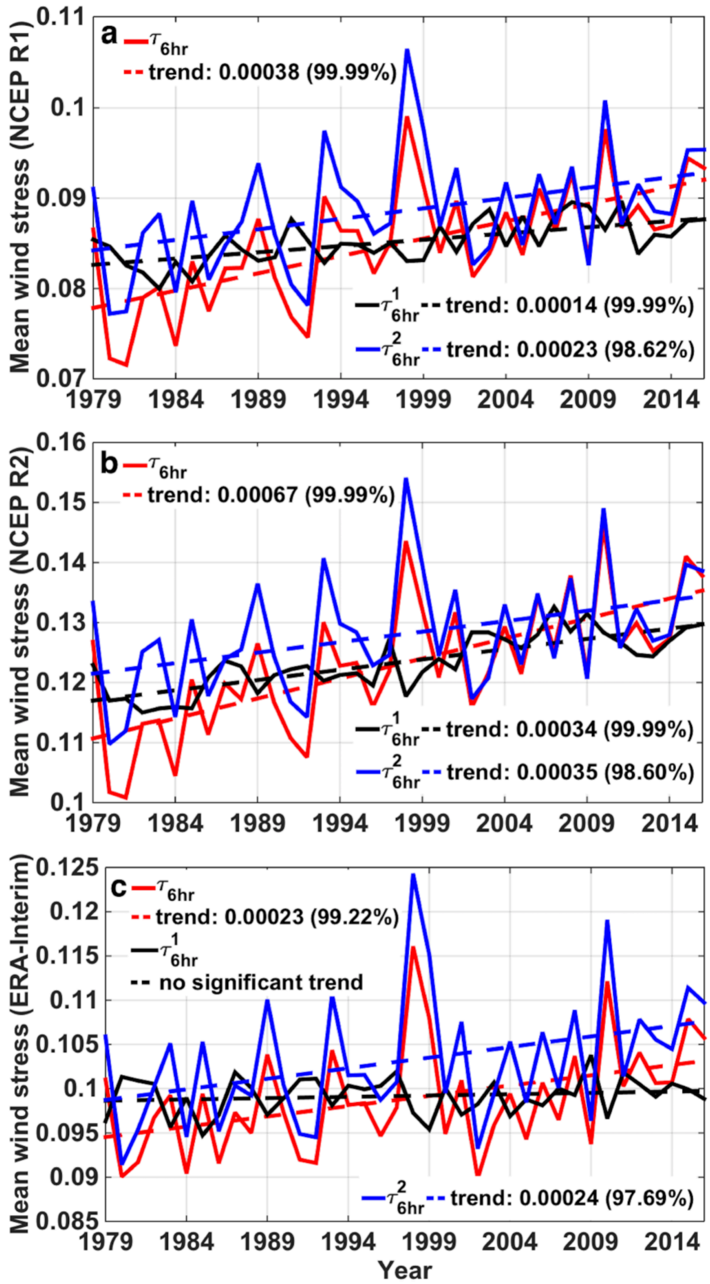

FIG. 10. Time series (red solid) and trend (red dashed) of SO wind stress averaged between 35^{o}S and 65^{o}S during 1979-2016 from (a) NCEP R1, (b) NCEP R2 and (c) ERA-Interim. Black lines are for wind stress obtained by randomizing the annual-mean winds and blue lines for that obtained by randomizing wind fluctuations. Percentages in brackets show statistical significance of the trends. Note that although the overall wind stress trends are positive when averaged between 35^{o}S and 65^{o}S, there are regions of negative trends, particularly between 35^{o}S and 45^{o}S (not shown).

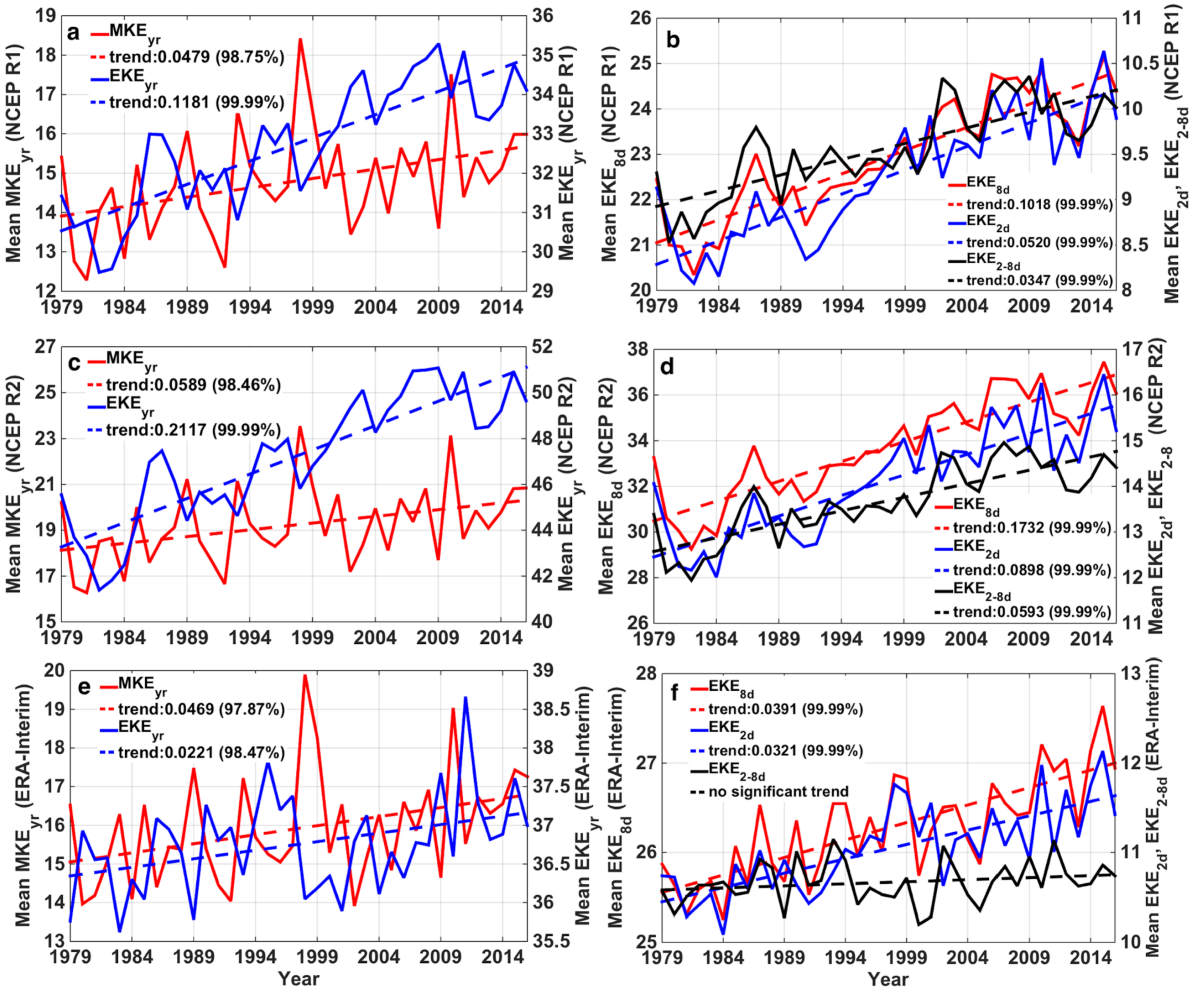

FIG. 11. Time series (solid) and trends (dashed) of $\mathrm{MKE_{yr}}$, $\mathrm{EKE_{yr}}$, $\mathrm{EKE_{8d}}$, $\mathrm{EKE_{2d}}$ and $\mathrm{EKE_{2-8d}}$ (m^2 s^{-2}) averaged between 35°S and 65°S during 1979-2016 from NCEP R1 (a-b), NCEP R2 (c-d) and ERA-Interim (e-f). Percentages in brackets show statistical significance of the trends.

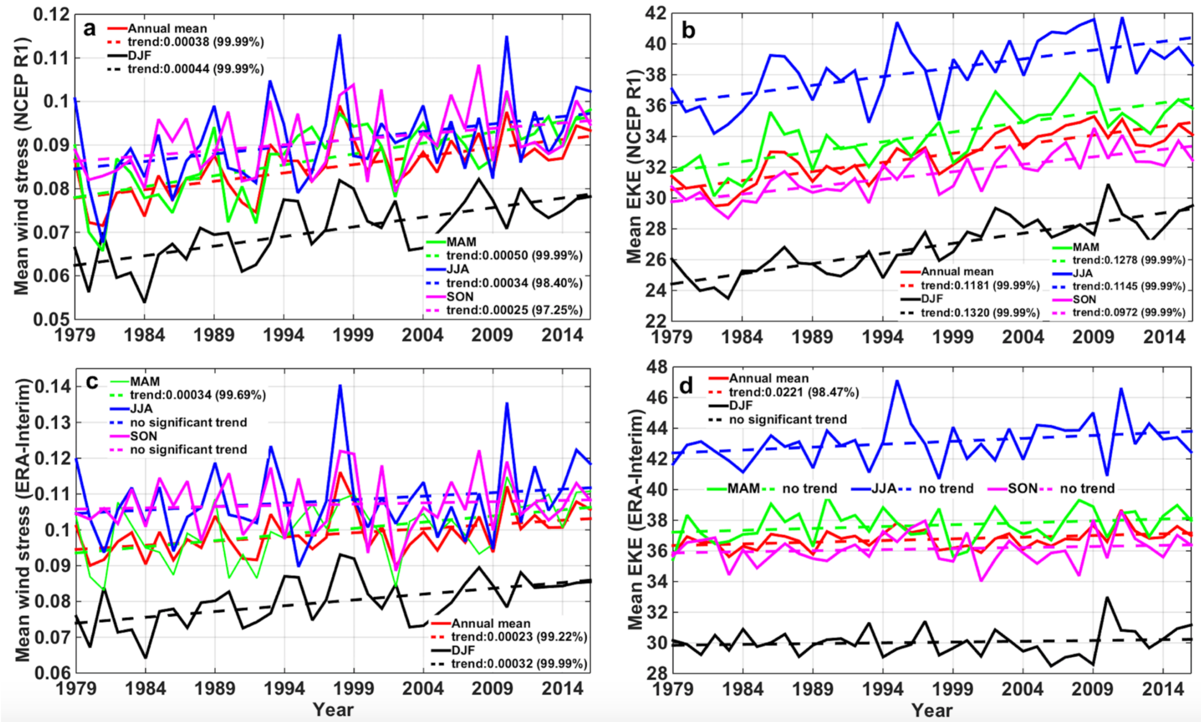

FIG. 12. Time series (solid) and trends (dashed) of the seasonal-mean τ_{6hr} (N m^{-2}, a and c) and EKE_{yr} (m^2 s^{-2}, b and d) averaged between 35°S and 65°S during 1979-2016 from NCEP R1 (a-b) and ERA-Interim (c-d). Percentages in brackets show statistical significance of the trends.